Turk J Chem
35 (2011) , 61 – 71.

doi:10.3906/kim-0905-42

Reaction dynamics of Br + HD: quantum wave packet on three potential energy surfaces

Qing SONG*, Wei-Long QUAN and Tian-Jun FENG
School of Mathematics, Physics & Software Engineering, Lanzhou Jiaotong University, Lanzhou, 730070, CHINA
e-mail: songqing@mail.lzjtu.cn, weilongq@mail.lzjtu.cn

Received 31.05.2009

The initial state-resolved reaction probabilities, reaction cross-sections, and rate constants of the reaction Br + HD are computed on 3 potential energy surfaces (denoted as e-LEPS, MB2, and MB3, respectively) by carrying out quantum time-dependent wave packet calculations. The results show that the reactivity of Br + HD on MB3 is much stronger than that on e-LEPS and somewhat weaker than that on MB2. Both of the vibrational and the rotational excitation of reagent HD enhance the reaction, which depends on the PESs and the strongest enhancement effects are on e-LEPS.

Key Words: Reaction Br + HD, time-dependent wave packet, reaction cross section

Introduction

$Br+H_2$ is of interest to study the electronic non-adiabatic effects since the vibration exciting energy of H_2 is very close to the split energy between $Br(^2P_{1/2})$ and Br $(^2P_{3/2})$.[1,2] Relative to the extensive research on the system H_2F and H_2Cl,[3–9] studies on system H_2Br are far from sufficient.

Several ab initio potential energy surfaces (PES), including e-LEPS,[10] MB2,[11,12] and MB3,[13] have been presented for the H_2Br system and we have studied the reaction dynamics of Br + H_2 on these PESs using the quantum time-dependent wave packet (TDWP) method.[14,15] Our calculations showed that MB3 was the most reliable PES among them because the reaction rate constant calculated on MB3 was in excellent agreement with experimental results, while that on e-LEPS was too small and that on MB2 was too large.

In this paper, we extend the TDWP calculation to the isotopic reaction Br + HD. The initial state-resolved reaction probabilities, reaction cross-sections, and rate constants are computed for the reaction Br

*Corresponding author

+ HD on the 3 potential energy surfaces mentioned above. The effects of HD ro-vibration excitation on the reaction dynamics are also examined.

Potential energy surfaces and calculations

Three PESs, e-LEPS, MB2, and MB3, were used to perform the quantum time-dependent wave packet calculation for the reaction Br + HD. Detailed information about these PESs has been reported in references 10-13 and can be found in the appendix; here we only discuss the main characteristics of these PESs. At the collinear geometries (Figure 1(a), (b) and (c)), e-LEPS, MB2 and MB3 are quite similar though the energy barrier of e-LEPS in this configuration is a little lower and thinner, but these PESs are very different at the T-shaped geometries (Figure 1(d), (e) and (f)). Firstly, a 'normal' reaction path, which is usually defined as the path along the gradient of potential energy from reactants to products, cannot be found on e-LEPS at the T-shaped configuration, while on MB3 and MB2 it is apparent at the T-shaped configuration. Secondly, the energy barrier on MB2 ($\sim$1.1 eV) is much lower than that on MB3 ($\sim$2.4 eV) and that on e-LEPS ($\sim$2.6 eV) at the T-shaped configuration. Thirdly, several artificial wells appear on MB2, but they are successfully eliminated from MB3.

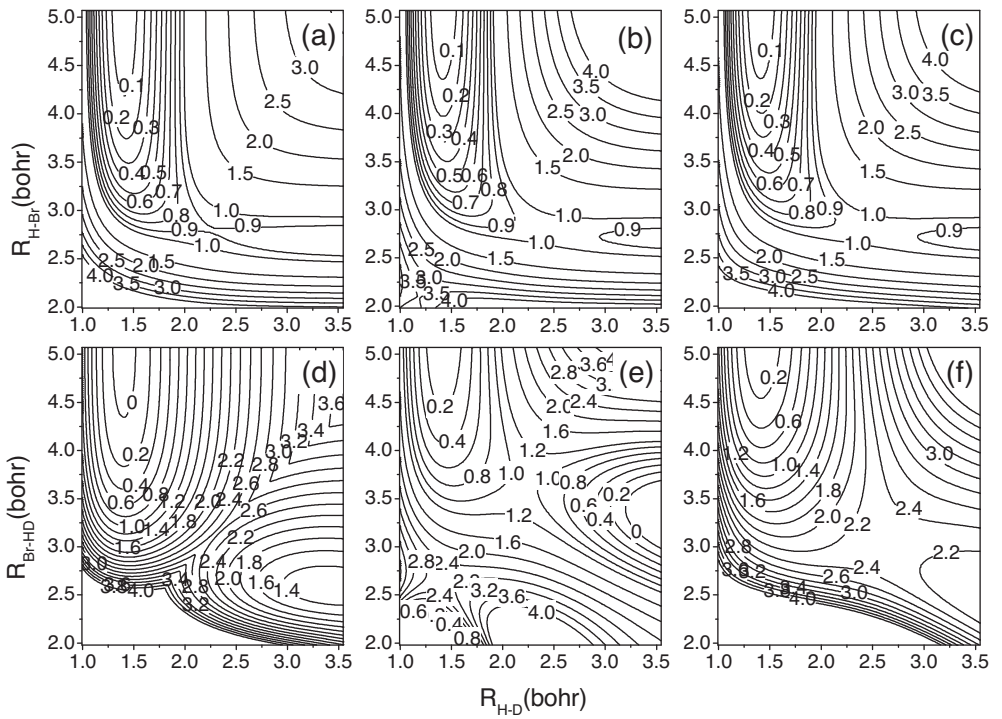

Figure 1. Contour plots of the potential energy surface. (a) e-LEPS, (b) MB2, (c) MB3 at the collinear configuration, (d) e-LEPS, (e) MB2, (f) MB3 at the T-shape configuration. The energy of Br + HD asymptote is selected as zero.

The time-dependent wave packet method, developed by Neuhauser and Baer,[16−18] and modified by Zhang,[19−22] is very useful to study chemical reaction dynamics, and has been well used in our previous

calculations on Br + H_2.[14,15] Here we only list the parameters used. In our calculations, a total of 185 sine functions (among them 90 for the interaction region) were employed for the translational coordinate R in a range of [0.5, 17.0] bohr. A total of 60 vibrational functions were employed for r in the range of [0.2 5.7] bohr. For the rotational basis we took $j_{\max} = 30$. The initial wave packet was centered at R = 16.2 bohr and with a width of 0.3 bohr and with an average translational energy of 0.9 eV. The total propagation time was 14,000 a.u. and the time step-size was 10 a.u.

Results and discussion

The reaction probability was firstly calculated on the above 3 PESs for the ground state reaction Br + HD ($v_0 = j_0 = 0$) and the results are shown in Figure 2. On all 3 PESs, the reaction probability of Br + HD ($v_0 = j_0 = 0$) increased with the translational energy. With the increasing total angular momentum, the reaction probability decreased and the reaction threshold shifted to higher energy. These are in agreement with the general feature of the reaction with a high barrier and can be considered as the result of the increasing centrifugal potential.

The differences of reaction probability on the 3 PESs are obvious. Firstly, the reaction probability increased very slowly with the translational energy on e-LEPS, but it became large abruptly near the onset of the reaction on MB2, and it increased gradually on MB3. Secondly, the reaction probability on e-LEPS was much smaller than that on MB3, and the reaction probability on MB2 was much larger than that on MB3.

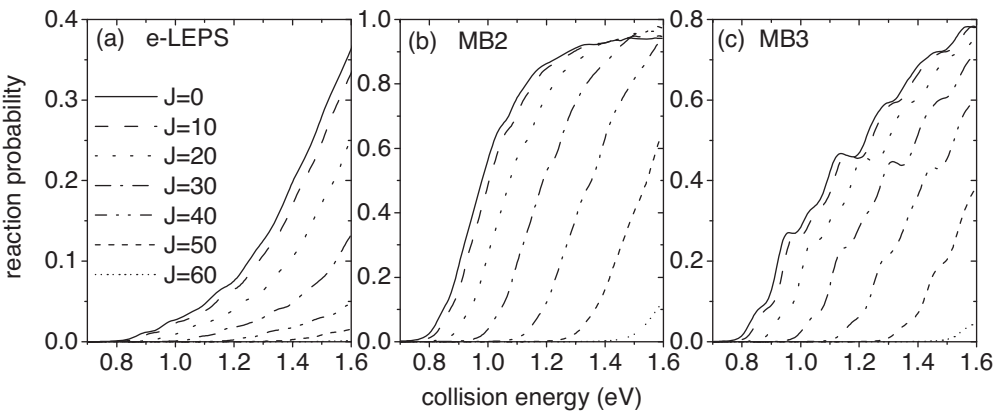

Figure 2. The J-dependent reaction probabilities for Br + HD (v= 0; j= 0) obtained on e-LEPS (a), MB2 (b), and MB3 (c) are shown as a function of the collision energy.

These differences can be resonated from the different features of the 3 PESs. Firstly, along the minimum energy path (which is just in collinear geometries for the reaction Br + HD), the energy barrier on MB2 and MB3 is almost identical and is much higher than that on e-LEPS. If the reaction Br + HD is dominated by the feature of the PES along the minimum energy path, it can be expected that the reactivity on e-LEPS is the strongest and the difference of the reactivity on MB2 and MB3 is very small. However, our calculations show that the reactivity on e-LEPS is the weakest one and the reactivity on MB3 is much stronger than that on MB3. These inconsistencies imply that the difference in Br + HD reactivity on the 3 PESs was not caused

by the PES feature near the collinear geometries. Secondly, for the e-LEPS PES, a high, abrupt energy barrier divides the product region from the reactant region and no appropriate path can be followed by the reaction at the T-shaped geometries. It means that when a Br atom perpendicularly approaches HD, the collision on e-LEPS is not reactive. Thirdly, for the MB2 and MB3 PES, the reaction path on both of them is apparent at T-shaped geometries, but the energy barrier on MB2, about 1.1 eV, was much smaller than that on MB3, about 2.4 eV. Therefore, the reactivity on MB2 was much stronger than that on MB3. Altogether, the reason for the differences in the reactivity of Br + HD on the 3 PESs is not the barrier along the minimum energy path, but the remarkable difference of them in the region far away from the minimum energy path.

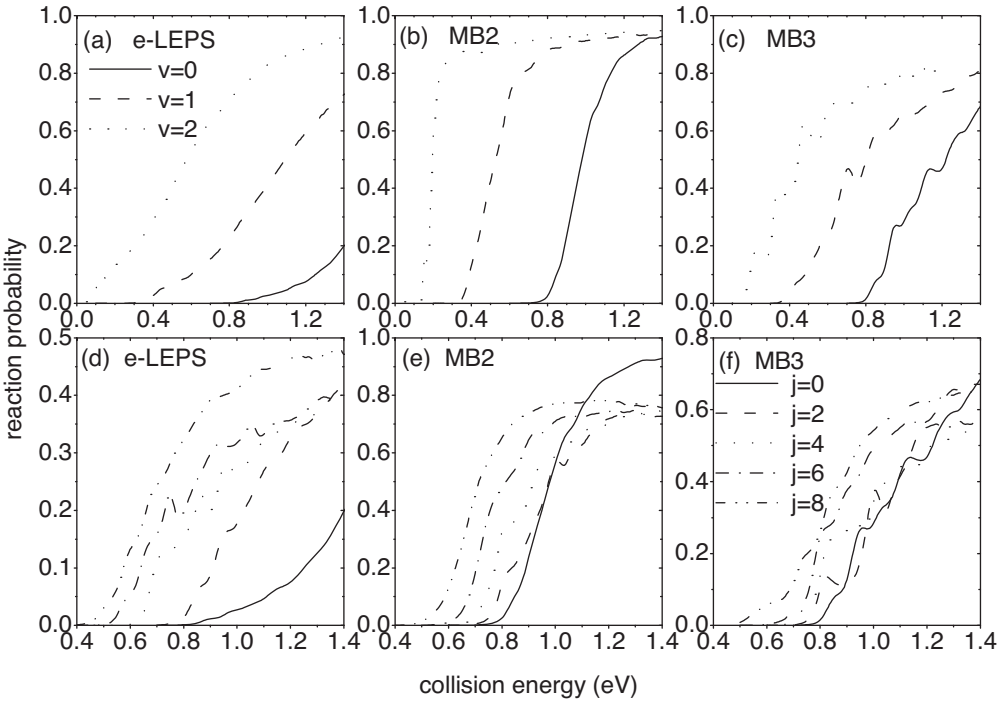

Figure 3. The reaction probabilities for Br + HD with different ro-vibrational states of HD are shown as a function of the collision energy. (a) e-LEPS, (b) MB2, and (c) MB3 for vibrations; (d) e-LEPS, (e) MB2, and (f) MB3 for rotations.

Similar calculations were then carried out for excited states of HD to investigate the effect of ro-vibrational excitation on the reactivity. As shown in Figure 3, on all the 3 PESs, the vibrational excitation of HD decreases the reaction threshold energy and thus significantly enhances the reaction (Figure 3 (a), (b) and (c)). The rotational excitation of HD also decreases the reaction threshold and enhances the reaction (Figure 3 (d), (e) and (f)), but its effect is much weaker than that caused by vibrational excitation. The reason for this trend is rooted in the fact that the vibration excitation affords much more energy for the reaction than the rotation excitation does.

Another interesting trend is that the enhancement effect of excitation on e-LEPS was more obvious than that on MB3 and MB2. To further understand this trend, the reaction probabilities are plotted as a function of the total energy (Figure 4); it shows that at the same total energy the reactivity on e-LEPS increases with the ro-vibrational excitation, but on MB2 and MB3 it decreases with the ro-vibrational excitation. This indicates

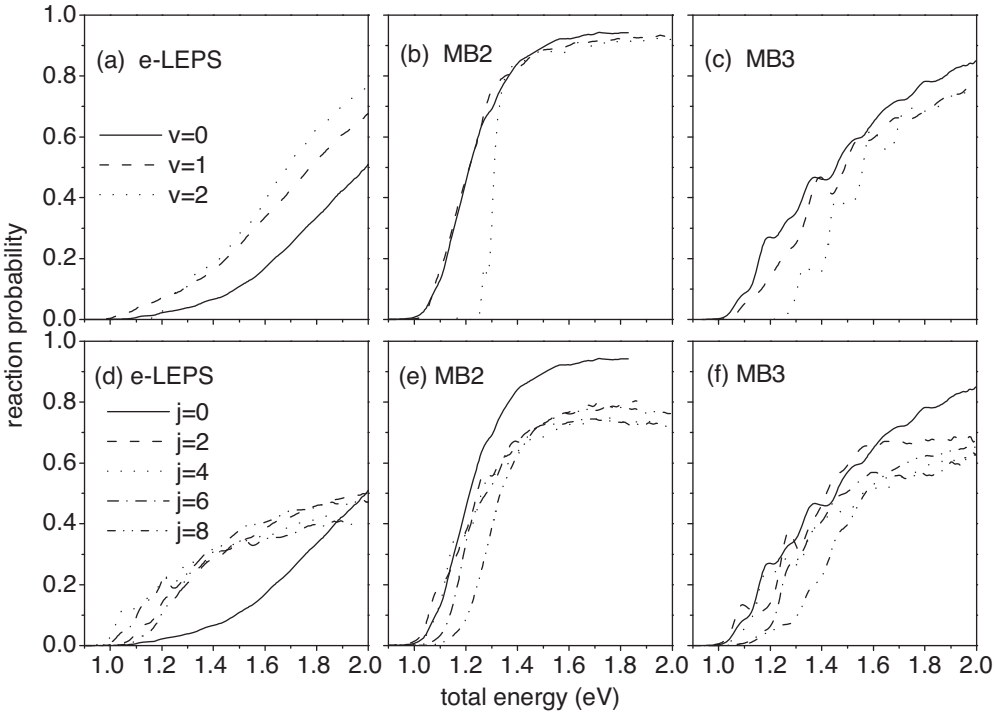

Figure 4. The reaction probabilities for Br + HD with different ro-vibrational states of HD are shown as a function of the total energy. (a) e-LEPS, (b) MB2, and (c) MB3 for vibrations; (d) e-LEPS, (e) MB2, and (f) MB3 for rotations.

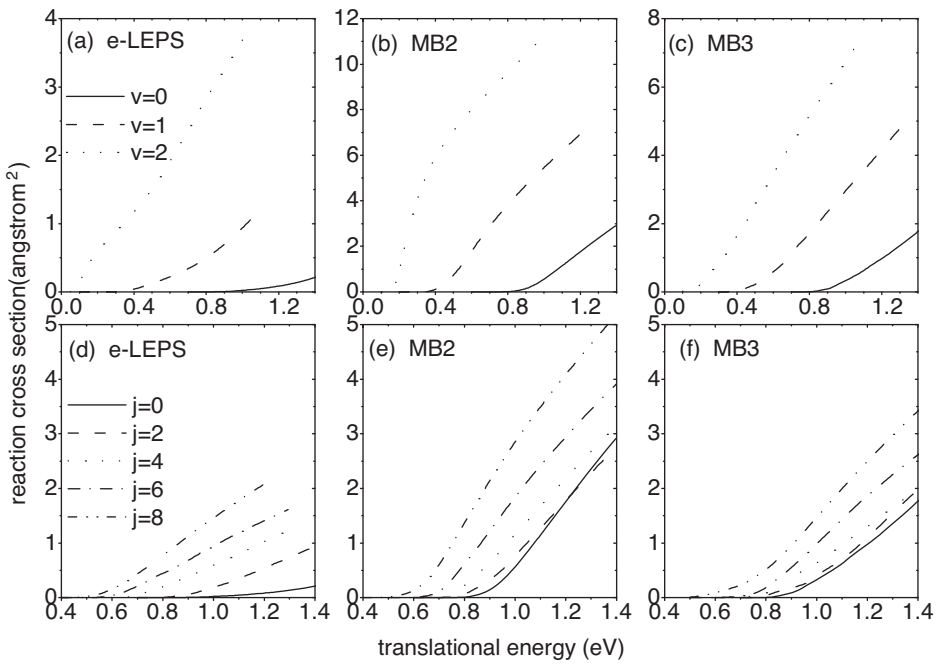

Figure 5. The reaction cross section of Br + HD with different ro-vibrational states of HD versus the collision energy. (a) e-LEPS, (b) MB2, and (c) MB3 for vibrational excitation and $j_0 = 0$. (d) e-LEPS, (e) MB2, and (f) MB3 for rotational excitation and $v_0 = 0$.

that at the same total energy putting more energy into ro-vibration is helpful to the reaction on e-LEPS, but on MB2 and MB3 it is harmful to the reaction. It also suggested that the transform efficiency of energy from ro-vibration into collision on these PESs is different. Noting that e-LEPS is the most anisotropic PES and MB2 is the most isotropic one. It seems that the ro-vibrational excitation is more helpful to the reaction on an anisotropic PES than on an isotropic one.

The reaction cross sections were then calculated by weighted-summing the reaction probabilities of all the total angular momentum up to a certain value and the results are shown as a function of the collision energy in Figure 5. Clearly, the reaction cross section on e-LEPS is much smaller than that on MB3, but the reaction cross section on MB2 is much larger than that on MB2. On all the 3 PESs, the reaction cross sections increase with the ro-vibrational excitation, but the increment on e-LEPS is larger than that on MB2 and that on MB3 and the effect of rotation is weaker than that of vibration. These are similar to the trend in the reaction probability and can be explained by the difference of PESs.

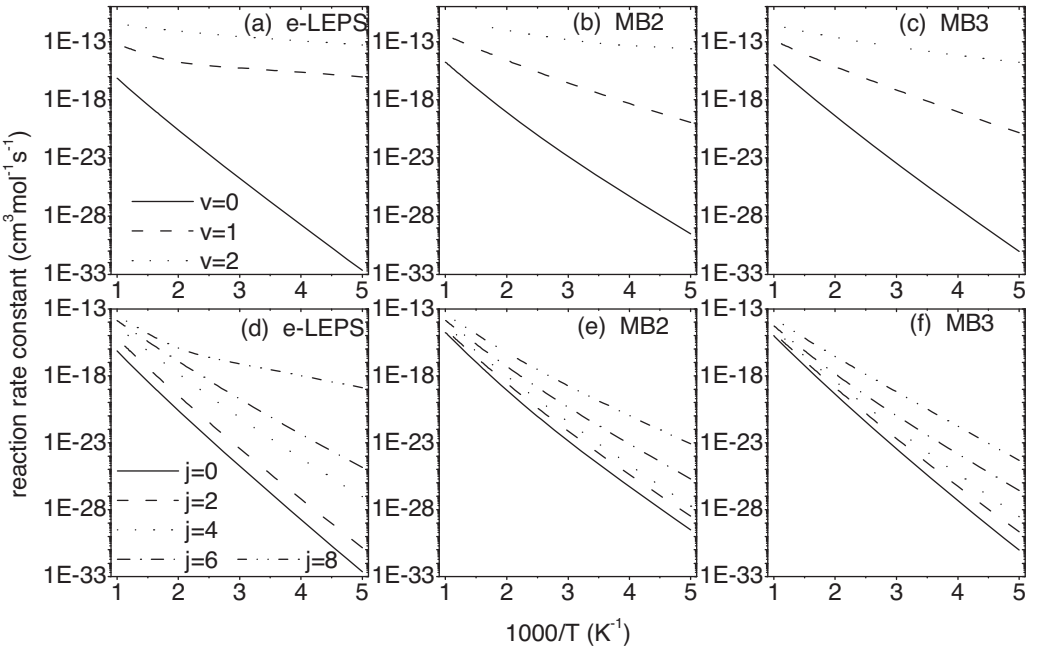

Figure 6. Semi-logarithmic plots of the rate constants for Br + HD with different ro-vibrational states of HD. (a) e-LEPS, (b) MB2, and (c) MB3 for vibrational excitation and $j_0 = 0$; (d) e-LEPS, (e) MB2, and (f) MB3 for rotational excitation and $v_0 = 0$.

The reaction rate constants were also calculated on the 3 PESs. As shown in Figure 6, the rate constant on e-LEPS is the smallest, and the rate constant on MB2 is the largest. The ro-vibrational excitation of HD increases the reaction rate constants on all the 3 PES, and again the increment on e-LEPS is much larger than that on MB2 and MB3, especially at low temperature. In each panel of Figure 5, the slope of the line decreased with the ro-vibrational excitation. It also indicates that the ro-vibrational excitations decrease the reaction threshold energy. The trends are similar to the reaction probabilities and the reaction cross sections, and the reasons have been discussed in previous paragraphs.

Conclusion

In the present study, the initial state-resolved reaction probabilities, cross sections, and rate constants were calculated for the reaction Br + HD on 3 different potential energy surfaces by carrying out quantum time-dependent wave packet calculations. From our calculation the following conclusions can be derived: (a) the reactivity of Br + HD depends on the PESs used. The smallest one is on e-LEPS, the largest one is on MB2, and that on MB3 is moderate; (b) the PES characteristics at the T-shaped geometries have a significant influence on the dynamics of the reaction Br + HD; (c) the ro-vibrational excitation enhances the reaction and the strongest enhancement is found to be on e-LEPS, which is the most anisotropic one of the 3 PESs. The above features are similar to those for the reaction Br + H_2 and can be explained by the different characteristics of the 3 PESs.

References

1. Takayanagi, T.; Kurosaki, Y. *J. Chem. Phys.* **2000**, *113*, 7158-7164.
2. Pomerantz, A. E.; Camden, J. P.; Chiou, A. S.; Ausfelder, F.; Chawla, N.; Hase, W. L.; Zare, R. N. *J. Am. Chem. Soc.* **2005**, *127*, 16368-16369.
3. Aquilanti, V.; Cavalli, S.; Simoni, A.; Aguilar, A.; Lucas, J. M.; Fazio, D. D. *J. Chem. Phys.* **2004**, *121*, 11675
4. Balucani, N.; Skouteris, D.; Cartechini, L.; Capozza, G.; Segoloni, E.; Casavecchia, P. *Phys. Rev. Lett.* **2003**, *91*, 013201(4 pages).
5. Skouteris, D.; Laganà, A. *J. Phys. Chem.* A. **2006**, *110*, 5289-5294
6. Ghosal, S. and Mahapatra, S. *J. Chem. Phys.* **2004**, *121*, 5740-5753.
7. Aquilanti, V.; Cavalli, S.; Fazio, D. D.; Volpi, A.; Aguilar, A.; Maria Lucas, J. *Chem. Phys.* **2005**, *308*, 237-253
8. Rusin, L. Y.; Toennies, J. P. *Phys. Chem. Chem. Phys.* **2000**, *2,* 501-506.
9. Skodje, R. T.; Skouteris, D.; Manolopoulos, D. E.; Lee, S.-H.; Dong, F.; Liu, K. *Phys. Rev. Lett.* **2000**, *85*, 1206-1209.
10. Lynch, G. C.; Truhlar, D. G.; Brown, F. B.; Zhao, J-G. *J. Phys. Chem.* **1995**, *99*, 207-225.
11. Kurosaki, Y.; Takayanagi, T. *J. Chem. Phys.* **2003**, *119*, 7838-7856.
12. Kurosaki, Y.; Takayanagi, T. *Chem. Phys. Lett.* **2005**, *406*, 121-125.
13. Kurosaki, Y. (private communication)
14. Quan, W. L.; Tang, P. Y.; Tang, B. Y. *Intel. J. Quant. Chem.* **2007**, *107*, 657-664
15. Quan, W. L.; Song, T.; Tang, B. Y. *Chem. Phys. Lett.* **2007**, *437*, 165-169.
16. Neuhauser, D.; Baer, M. *J. Chem. Phys.* **1989**, *90*, 4351-4355.
17. Neuhauser, D.; Baer, M. *J. Chem. Phys.* **1989**, *91*, 4651-4657.
18. Baer, M.; Neuhauser, D.; Oreg, Y. *J. Chem. Soc., Faraday Trans.* **1990**, *86*, 1721-1728.
19. Zhang, D. H.; Zhang, J. Z. H. *J. Chem. Phys.* **1994**, *101*, 1146-1156.
20. Zhang, D. H.; Zhang, J. Z. H. *J. Chem. Phys.* **1994**, *101*, 3671-3678.
21. Dai, J.; Zhang, J. Z. H. *J. Phys. Chem.* **1996**, *100*, 6898-6903.
22. Zhang, D. H.; Lee, S. Y. Baer, M.; *J. Chem. Phys.* **2002**, *112*, 9802-9809.

Appendix: the potential functional forms and the parameter

A. e-LEPS potential functions[10]

Lynch chose the extended London-Eyring-Polanyi-Sato (e-LEPS) functional form to represent the global H2Br potential energy surface because it is simple and it provides a good representation of the H + HBr abstraction region of the potential, and to predict the H-Br-H exchange barrier a localized 3-center term was also used. That is, the total potential energy was written as:

$$E = E_{e-LEPS} + E_{3C} \tag{1}$$

where the e-LEPS potential is

$$E_{e-LEPS} = \frac{Q_1}{1+\Delta_1} + \frac{Q_2}{1+\Delta_2} + \frac{Q_3}{1+\Delta_3} - \left\{ \frac{1}{2} \left[\left(\frac{J_1}{1+\Delta_1} - \frac{J_2}{1+\Delta_2} \right)^2 + \left(\frac{J_2}{1+\Delta_2} - \frac{J_3}{1+\Delta_3} \right)^2 + \left(\frac{J_3}{1+\Delta_3} - \frac{J_1}{1+\Delta_1} \right)^2 \right] \right\}^{\frac{1}{2}} \tag{2}$$

in which

$$Q(r) = \frac{1}{2}[E_{AM}(r) + E_M(r)], \quad J(r) = -\frac{1}{2}[E_{AM}(r) - E_M(r)] \tag{3}$$

and

$$E_M(r) = D_e \left\{ \exp[-2\beta(r - r_0)] - 2\exp[-\beta(r - r_0)] \right\} \tag{4}$$

$$E_{AM}(r) = \frac{D_e}{2} \left\{ \exp[-2\beta(r - r_0)] + 2\exp[-\beta(r - r_0)] \right\} \tag{5}$$

The Sato parameters in (2) were fitted as

$$\Delta_{HH} = \frac{A_{HH} R_{HH}^2}{R_{0,HH}^2 + R_{HH}^2} \tag{6}$$

$$\Delta_{HBr} = 0.1675 + R_{Br-HH}^2 \left[\frac{\sin^2 \phi}{R_{2,HBr}^2} + \frac{\sin^4 \phi}{R_{4,HBr}^2} \right] \tag{7}$$

The localized 3-center term in (1) was defined as

$$E_{3C} = A_1 f_1(R_1, R_3) f_2(R_1, R_3) f_3(R_1, R_2, R_3) f_1(\Phi) \tag{8}$$

and

$$f_1 = \exp[-A_2(R_1 + R_3)] \tag{9}$$

$$f_2 = \exp[-A_3(R_1 - R_3)^2] \tag{10}$$

$$f_3 = \exp[-A_4(R_1 + R_3 - R_2)^2] \tag{11}$$

$$f_4 = 1 + A_5 \sin^2(\pi - \Phi) + A_6 \sin^8(\pi - \Phi) \tag{12}$$

where R_1 and R_3 were the 2 H-Br bond lengths, R_2 was the H-H bond length, and Φ was the H-Br-H bond angle. The parameters for Lynch's e-LEPS potential energy surface are listed in Table 1.

Table 1. Parameter in e-LEPS potential energy surface for BrH_2.[10]

parameter	value	parameter	value
$D_{e,HH}$	129.28 kar/mol	A_{HH}	0.291230499
$D_{e,HBr}$	90.60 kar/mol	A_1	1.67457884 hartrees
β_{HH}	1.028224 a_0^{-1}	A_2	0.709518875 a_0^{-1}
β_{HBr}	0.95688859 a_0^{-1}	A_3	0.187582679 a_0^{-2}
$R_{0,HH}$	4.99160974	A_4	0.243517074 a_0^{-2}
$R^2_{2,HBr}$	260.2386 a_0^2	A_5	0.204145206
$R^2_{4,HBr}$	374.6533 a_0^2	A_6	2.57833022

B. Many body potential functions[11−13]

Kurosaki represented the H_2Br potential energy surface as a sum of three 2-body terms and a 3-body term:

$$V_{ABC} = V_{AB} + V_{BC} + V_{AC} + V_{ABC} \tag{13}$$

where the diatomic potential was written as a sum of 2 terms, one representing the short-range and the other the long-range potential

$$V_{AB} = \frac{c_0 \exp(-\alpha_{AB} R_{AB})}{R_{AB}} + \sum_{i=1}^{N} c_i \rho_{AB}^i \tag{14}$$

where $\rho_{AB} = R_{AB} \exp(-\beta_{AB} R_{AB})$ The 3-body term was written as

$$V_{ABC} = \sum_{i,j,k}^{M} d_{ijk} \rho_{AB}^i \rho_{BC}^j \rho_{AC}^k \tag{15}$$

Table 2. Parameters (all in atomic unit) for 2-body terms in MB2 and MB3 potential energy surface for BrH_2.[11−13]

BrH $\alpha_{BrH} = 1.300019$ $\beta_{BrH} = 0.8215065$		HH $\alpha_{HH} = 2.290247$ $\beta_{HH} = 1.114820$	
i	c_i	i	c_i
0	16.4925601097	0	1.07149880186
1	-0.100804587537	1	-4.43942685561
2	3.80660091133	2	-8.80729271054
3	-121.726869794	3	59.4497405752
4	846.612357698	4	-251.263513125
5	-2969.26582982	5	666.833061366
6	5253.52346684	6	-1012.68262574
7	-3822.47924058	7	664.881960814

where the definition of ρ_{BC} and ρ_{AC} were similar to that of ρ_{AB}, the indices i, j, k vary from zero to a maximum value such that

$$i + j + k \neq i \neq j \neq k \tag{16}$$

$$i + j + k \leq 7 \tag{17}$$

The parameters for many-body (MB) type potential energy surface of H_2Br are listed in Tables 2-4.

Table 3. Parameters (all in atomic unit) for 3-body terms in MB2 PES for BrH_2.[11,12]

$\beta_{BrH} = 0.7702996296241558, \quad \beta_{HH} = 0.8885476532053922$			
ijk	d_{ijk}	ijk	d_{ijk}
110 (011)	33.00008192349735	330 (033)	5408.865878262551
101	-1.556257132154942	303	-819.833781737636
111	-532.0047852936391	411 (114)	5348.045141556771
210 (012)	-347.6845970526057	141	-3631.584087713839
201 (102)	-38.33956334821166	420 (420)	5361.38310495602
021 (120)	-104.0795990135922	402 (204)	3298.387023519796
211 (112)	1826.987608247834	042 (240)	-1960.852379584685
121	2782.322859247484	510 (015)	551.713329119144
220 (022)	1428.563467221439	501 (105)	2323.646786579277
202	221.6365234887598	051 (150)	460.8249482308287
310 (013)	1266.039746598514	322 (223)	1619.963636896733
301 (103)	524.0959891518279	232	-24482.47957681645
031 (130)	-113.9206440488047	331 (133)	-7938.718811643916
221 (122)	-9603.174187170858	313	-14716.26709004237
212	-3602.731750473537	421 (124)	-5365.133853793977
311 (113)	-2557.780326053869	412 (214)	7364.705097935082
131	-2787.264958829719	142 (241)	-958.1731724343498
320 (023)	-5248.166959126407	430 (034)	-6635.090821569927
302 (203)	-996.4917570272021	403 (304)	1675.433025593487
032 (230)	-664.5679808820898	043 (340)	1669.789280684623
410 (014)	-1742.371308551505	511 (115)	-7234.173357871872
401 (104)	-1945.078615453716	151	4143.78350507165
041 (140)	338.0649508353537	520 (025)	1301.621660375189
222	16716.57243997489	502 (205)	-4470.878331246091
321 (123)	7898.683638767822	052 (250)	36.99057887531475
312 (213)	1165.232750769003	610 (016)	-29.23802975964097
132 (231)	13290.30376316055	601 (106)	-83.5077479096243
		061 (160)	-628.5280860524688

Table 4. Parameters (all in atomic unit) for 3-body terms in MB3 potential energy surface for BrH_2.[13]

$\beta_{BrH} = 0.7900010000000001, \quad \beta_{HH} = 0.8100010000000001$			
ijk	d_{ijk}	ijk	d_{ijk}
110 (011)	18.28021095377481	330 (033)	1484.134438202093
101	-22.45999474630225	303	-6193.45782365261
111	-170.929236707066	411 (114)	1926.931343384952
210 (012)	-145.9602725140234	141	-1106.057227928166
201 (102)	160.3279893886734	420 (420)	-316.6294825866724
021 (120)	-58.87929973361864	402 (204)	-494.132269234331
211 (112)	628.4896413943582	042 (240)	-1525.741083276035
121	800.402519443588	510 (015)	-421.1577822321706
220 (022)	567.1715520729363	501 (105)	2218.281555394696
202	-1255.641840908673	051 (150)	-99.76864833730021
310 (013)	263.2323843248279	322 (223)	-5046.156460665228
301 (103)	-145.4659693440287	232	-1174.179632364796
031 (130)	-34.4488090159785	331 (133)	-4324.789614708248
221 (122)	-3739.14996052205	313	21689.97921123599
212	1777.829109371704	421 (124)	739.4461702705396
311 (113)	-1493.783341982146	412 (214)	-6700.199165995243
131	-482.4981837212854	142 (241)	-1308.825488800643
320 (023)	-1440.229967445454	430 (034)	-4046.819848206767
302 (203)	2689.558126279356	403 (304)	3347.262182660867
032 (230)	60.5755756112974	043 (340)	2750.08412430465
410 (014)	296.4322400891715	511 (115)	105.8718623613522
401 (104)	-1080.7887888646	151	1631.827773684873
041 (140)	213.7955017269666	520 (025)	3461.927886937204
222	5351.279480174273	502 (205)	-2486.49980464883
321 (123)	5534.408631911115	052 (250)	232.6560274339618
312 (213)	-4618.836748549839	610 (016)	-1145.267989233143
132 (231)	3701.114964756824	601 (106)	-469.4948333693502
		061 (160)	-3.584765922490625